Research Article

Parametric design for the valve seat of a high-temperature and high-pressure valve inside wind tunnels

Fengwei HOU[1], Haifeng SHU[1], Binbin WU[2], Chengliang YU[2], Zhehui MA[3], Wenqing LI[4✉], Jinyuan QIAN[3]

[1]*Hypervelocity Aerodynamics Institute, China Aerodynamics Research and Development Center, Mianyang 6210000, China*
[2]*Shanghai Koko Valve Group Co., Ltd., Shanghai 201802, China*
[3]*Institute of Process Equipment, Zhejiang University, Hangzhou 310027, China*
[4]*State Key Laboratory of Fluid Power and Mechatronic Systems, Zhejiang University, Hangzhou 310058, China*

Abstract: The high-temperature and high-pressure valve is the key equipment of the wind tunnel system; it controls the generated high-temperature and high-pressure gas. In order to reduce the adverse impact of high-temperature and high-pressure gas on the strength of the valve body, a cooling structure is set on the valve seat. This can significantly reduce the temperature of the valve body and seat. The effect of its structure on the cooling characteristic and stress of valve seat is studied and six main parameters that can completely describe the geometry of the cooling structure are proposed. The central composite design method is used to select sample points and the multi-objective genetic algorithm (MOGA) method is used for structural optimal design. Based on these, a modification method according to the main parameters for the valve seat is proposed. Results show that the cooling structure weakens the pressure bearing capability of the valve seat. Among the six main parameters of the valve seat, the distance from the end face of the lower hole to the Z-axis and the distance from the axis of the lower hole to the origin of the coordinates have the most obvious effect on the average stress intensity of the valve seat. An optimum design value is proposed. This work can provide a reference for the design of high-temperature and high-pressure valves.

Key words: Control valve; wind tunnel; valve seat; optimization; stress

1 Introduction

The wind tunnel test is one of the most important means of aerodynamics research in the aerospace field. It simulates the airflow around an aircraft or object by generating and controlling gas. It provides reliable reference data for aircraft design and testing (Formato et al., 2018; Yu et al., 2018; Shitolé et al., 2024; Achuthan et al. 2021). A high-temperature and high-pressure valve (HTHPV) is the key equipment of the wind tunnel test system. It works in a high-temperature and high-pressure environment and its main function is to control high-temperature and high-pressure gas in the wind tunnel system (Armijo et al., 2022; Zhou et al., 2022; Aliyeva et al., 2023;

✉ Wenqing LI, liwenqing@zju.edu.cn

(iD) Wenqing LI, https://orcid.org/0000-0001-6228-4772

Morales et al., 2023). Due to the high-temperature and high-pressure conditions, the valve body must have an excellent pressure-bearing capacity. If the structural design of the valve body is not efficient it may negatively affect the life span of the valve and cause economic loss and even casualties. Therefore, it is hard to overstate the importance of structure optimization of the valve body for a HTHPV to assure its reliability under extreme conditions (Bryk et al., 2022; Grice et al., 2022).

Thermal stress greatly impacts the pressure-bearing capacity of valves under high-temperature and high-pressure conditions (Shul'zhenko et al., 2021; Li et al., 2022; Sundararaj et al., 2022; Qian et al., 2023; Deng, 2022). The influencing mechanism of thermal stress on valve strength have been considered through experiment (Jawwad et al., 2019), numerical simulation (Bryk, 2022) and theoretical calculation (Hwang et al., 2020). Li et al. (2022) analyzed the valve body stress in the opening process of a feed-water valve by the

thermo-fluid-solid coupling method and measured the variation of thermal stress with time. Sun et al. (2021) studied the impact stress of the valve seat at the moment of rapid collision to prevent drawback, and then optimized the valve seat according to a response surface methodology combined with multi-objective optimization. Fersaoui et al. (2022) evaluated the effect of the thermo-mechanical boundary on the stress of the valve and calculated the thermal stress based on the temperature gradient of each component. Zhang et al. (2021) conducted thermal and structural analysis under transient thermal shock conditions using the thermal-fluid-structure coupling model They found that, rather than the pressure, thermal stress is the main source of stress causing overload accidents in nuclear power plants. Jalali et al. (2019) analyzed fatigue and crack in the stop valve body, and compared the stress concentration points obtained with the real coordinates of the crack so as to evaluate the reliability of the valve body.

Structural optimization is an effective way to improve the performance of the valve (Qi et al., 2021; Bao et al., 2022). Finding the optimal structural parameters of the valve through relevant optimization algorithms has attracted the attention of many researchers (Kunčická et al., 2022; Li et al., 2022). Zong (2022) et al. proposed a dimensionality-reduced computational fluid dynamics modeling method, selecting three structural parameters as design variables for structural optimization. Taking a Tesla valve as the research object, Wang et al. (2022) conducted optimization design, with two structural parameters as input variables and mixing efficiency and pressure drop as output parameters. Cao et al. (2022) focused on the nonlinearities and parameter uncertainties of a main pressure regulating valve, improving pressure regulation performance using parameters optimization and control methods. Zhang et al. (2022) used a new multi-objective gravitation search algorithm with non-dominated screening and chaos mutation to optimize the pressure regulating valve and revealed the relationship between multiple parameters of the valve. Lin et al. (2022) analyzed the effect of seal parameter on seal contact performance of the charge valve and improved the uniformity of the sealing surface by structural optimization. Wang et al. (2021) replaced the Kriging model with the response surface method for greater accuracy and

established a combined surrogate model to solve the optimization problem of a butterfly valve.

The above research indicates that reducing the thermal loading is beneficial for improving the bearing pressure ability of HTHPV. The most common way of heat insulation is to install material with ultra-low thermal conductivity, which prevents the contact between high-temperature fluid and the inner surface of the valve. The thermal shock of high-temperature fluid on the valve body is not completely eliminated by this method, which leads to increasing temperature of the valve. This article proposes insulation with a cooling structure. The cooling performance is significantly better than that from installing material with ultra-low thermal conductivity.

The HTHPV studied in this paper is insulated with asbestos between the flow channel of the valve body and the high-temperature and high-pressure gas. The valve body is thus unaffected by high-temperature and high-pressure loads. The temperature of the valve seat increases significantly as the seat is in direct contact with the high-temperature and high-pressure gas, amd leads to the possibility of creep or even structural failure in the seat. Therefore, a cooling structure is required inside the seat, where coolant can be introduced. The main research purpose of this paper is to improve the cooling efficiency and structural strength for the valve seat considering the cooling arrangements. The temperature of the valve seat with different cooling structures under steady-state condition is analyzed by a numerical simulation method and the thermal stress of the valve seat is calculated by the thermal-solid coupling method. The cooling structure is represented by six main structure parameters, which are set as independent variables. The average temperature and average thermal stress are selected as target variables. The response surface optimization method is conducted to determine the optimal structure parameters of the valve seat, for the best cooling performance and the lowest stress level in it. This work can provide a reference for the design of HTHPV in future.

2 Method description

2.1 Geometric model

Fig. 1 shows the structure of the high-temperature and high-pressure valve (HTHPV), whose size is the same as that of the actual product in the wind tunnel. HTHPV mainly consists of six parts: valve cover, valve stem, valve core, valve seat, valve body and inner pipe. The diameter of the inlet and outlet pipes for the HTHPV is 65 mm. The thermal insulation material is arranged between the valve body and the inner pipe and the cooling structure is set both in the valve body and valve seat and can reduce effectively the temperature of the valve body and valve seat. In this work, the XOZ plane is set on the symmetry plane of the valve body, as shown in Fig.1. In order to reduce the influence of boundary stress on the calculation results, pipes are added at the inlet and outlet of the HTHPV. The origin of coordinates is set at the intersection of axis of the inlet pipe and the outlet pipe.
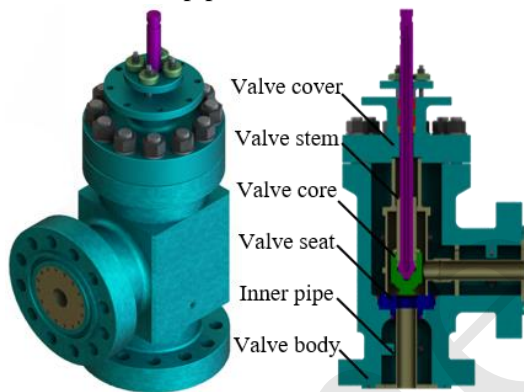

Fig. 2 Geometric model of the valve seat

2.2 Mesh and boundary condition

The mesh of the geometry of the HTHPV is carried out by MESH software in ANSYS WORK-BENCH (Canonsburg PA USA). The mesh of the HTHPV is shown in Fig.3. The sweep method is selected to mesh the inlet pipe and outlet pipe, whose grid size are both set to 12 mm. A tetrahedron grid is used to generate the mesh of the valve body, valve cover, valve seat and inner pipe. Gird sizes of the valve seat, inner pipe, valve body and valve cover are 4mm, 7mm and 12mm respectively with 871070 elements and 1328162 nodes. The contact type between components is bonded. The properties of solid materials are obtained from ASME BPVE.II.D.M -2021, and are listed in Table 1.

Fig. 1 Geometric model of high-temperature and high-pressure valve in wind tunnel

When the valve is closed, the valve core comes into close contact with the seat along the circumferential direction with no gap between them under preload. The valve seat, welded to the valve body, is connected with the inner pipe and valve core, which includes eight groups of cooling structures along the circumferential direction. Six key parameters of the cooling structure are selected to study the cooling performance. As shown in Fig.2, P_1 is the diameter of the upper round groove, P_2 is the diameter of the shear hole, P_3 is the distance from the center of the shear hole to the Z-axis, P_4 is the distance from the end face of the lower hole to the Z-axis, P_5 is the diameter of the lower hole, P_6 is the distance from the axis of the lower hole to the origin of the coordinates. The above six parameters completely describe the geometric characteristics of the cooling structure.
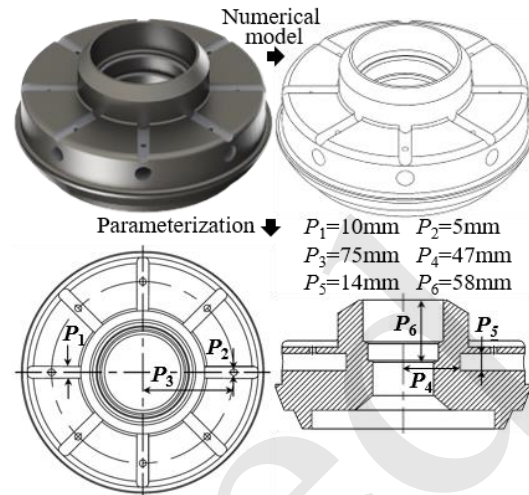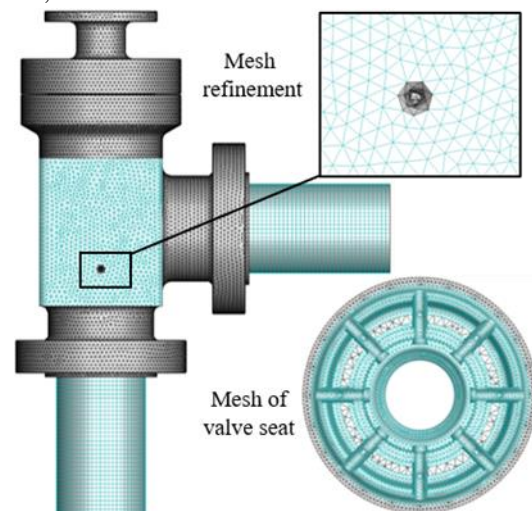

Fig. 3 Mesh of the HTHPV

Table 1 Measured data of the experiments in five states

Number	Part	Material
1	Valve cover	ASTM A182 F304
2	Valve stem	X-718/GH3128
3	Valve core	X-718/GH3128
4	Valve seat	NS3103/310S
5	Inner pipe	NS3103/310S
6	Valve body	ASTM A182 F304

As shown in Fig.4, there are three main boundary conditions for the temperature calculation for the HTHPV. The contact surface of the valve seat and inner pipe with the high temperature gas is regarded as a convection boundary, the temperature is 600 ℃ and the coefficient is 1000 W/m² ·℃. The surface of the cooling structure is regarded as a convection boundary, the temperature is 22 ℃ and the coefficient is 4500 W/m² ·℃, and is calculated by the Dittus-Boelter Equation. This equation is the longest and most commonly used correlation for forced convection inside pipelines.

$$Nu_f = 0.023\,\mathrm{Re}_f^{0.8}\,\mathrm{Pr}_f^n, \tag{1}$$
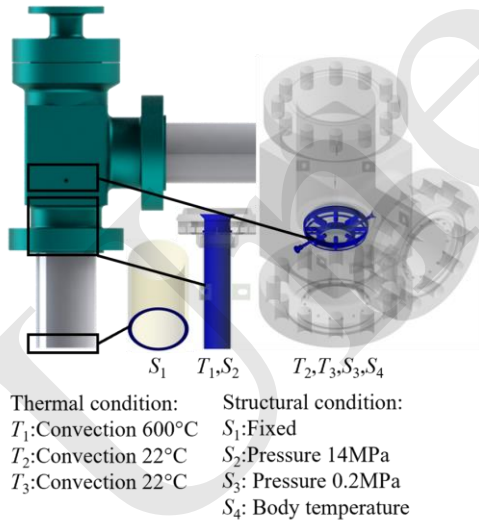
Fig. 4 Boundary conditions of the HTHPV

In this equation, Nu is the Nusselt Number; Re is the Reynolds Number; Pr is the Prandtl Number; when the fluid is heated, $n=0.4$, when the fluid is cooled, $n=0.3$. The calculation equation for the Nusselt Number is as follows:

$$Nu = \frac{hl}{\lambda}, \tag{2}$$

In this equation, h is the convective heat transfer coefficient, λ is the thermal conductivity coefficient, l is the characteristic length.

The calculation equation for the Reynolds Number is as follows:

$$\mathrm{Re} = \frac{ul}{v} \tag{3}$$

In this equation, u is the fluid velocity, v is the kinematic viscosity.

The external surface of the HTHPV is regarded as the convection boundary, the temperature is 22 ℃ and the coefficient is 15 W/m² ·℃. For the structural calculation of the HTHPV, there are four main boundary conditions. The contact surface of the valve seat and inner pipe with the high temperature gas is set as the pressure boundary, with a value of 14 MPa. The surface of the cooling structure is set as the pressure boundary; the value is 0.2 MPa. The end surface of the down pipe is a fixed boundary. The temperature distribution n the HTHPV is introduced into the later stress analysis for the HTHPV.

2.3 Optimization method

In this work, as shown in Table 2, the parameters P_1, P_2, P_3, P_4, P_5, P_6 are set as input parameters, and the parameters P_7, P_8, P_9, P_{10}, P_{11}, P_{12}, P_{13} are set as output parameters. P_7 is the average temperature of the valve seat, in ℃; P_8 is the maximum temperature of the cooling surface for the valve seat, in ℃; P_9 is the average temperature of the cooling surface for the valve seat, in ℃; P_{10} is the maximum stress intensity of the valve seat, in MPa; P_{11} is the average stress intensity of the valve seat in MPa; P_{12} is the maximum stress intensity of the cooling surface for the valve seat, in MPa; P_{13} is the average stress intensity of the cooling surface for the valve seat in MPa. In order to fully analyze the effect of structural parameters on cooling and bearing pressure capacity, the selection range of input parameters is the limit that can construct geometric entities. In order to ensure structural integrity, parameter values are set as shown in table 3. This paper takes the minimum values of P_7 and P_{11} as the goal of optimization. The central composite design method is selected for experiments. It provides effective information about experimental variables and experimental errors with

minimal test cycles; 45 samples are generated. The screening method is selected for optimization. The genetic aggregation is selected to fit the response surface. A multi-objective genetic algorithm (MO-GA) method is used for structural optimization design, as a classic multi-objective optimization algorithm. Its basic aim is to solve multi-objective optimization problems within the framework of a genetic algorithm; it uses techniques such as fitness sharing, Pareto front ranking, and crowding distance. The main steps of MOGA are eight: population initialization, fitness calculation, Pareto front sorting, crowding distance calculation, selection operation, crossover and mutation operation, population update, and terminination condition.

Table 2 Meanings of input parameters and output parameters

Type	Number	Parameter	Name
input parameters	1	P_1	diameter of the upper round groove
	2	P_2	diameter of the shear hole
	3	P_3	distance from center of shear hole to the Z-axis
	4	P_4	distance from end face of lower hole to the Z-axis
	5	P_5	diameter of the lower hole
	6	P_6	distance from the axis of the lower hole to the origin of coordinates
output parameters	7	P_7	average temperature of the valve seat
	8	P_8	maximum temperature of the cooling surface
	9	P_9	average temperature of the cooling surface
	10	P_{10}	maximum stress intensity of the valve seat
	11	P_{11}	average stress intensity of the valve seat
	12	P_{12}	maximum stress intensity of cooling surface
	13	P_{13}	average stress intensity of the cooling surface

Table 3 Value range of structural parameters of valve seat

Number	Parameter	Initial value	Range
1	P_1	10 mm	9–14 mm
2	P_2	5 mm	2–8 mm
3	P_3	75 mm	65–85 mm
4	P_4	47 mm	35–50 mm
5	P_5	14 mm	8–14 mm
6	P_6	58 mm	43–58 mm

2.4 Verification of results

A theoretical calculation is carried out to verify the accuracy of the numerical results. The inner pipe of HTHPV is selected as the object. Its geometry is relatively regular. The inlet pipeline of the valve is considered as a thin-walled cylinder under a uniform internal pressure environment and its stress is calculated by the force balance principle.The radial stress (X-axis) of the inlet pipe is selected as the reference index. The inner wall radius of the inner pipe is r_1=32.5 mm, the outer wall radius of the inner pipe is r_2=36.5 mm. The stress intensity of the inner pipe is calculated as follows:

$$\sigma = \frac{PD}{2t} = \frac{14 \times 69}{2 \times 4} = 120.5 \text{MPa} \tag{4}$$

For the numerical calculation, six paths are established and average stress values are obtained. Fig. 5 shows the comparison between numerical results and theoretical results. The maximum stress for numerical calculation is 123.51 MPa, with a relative error between numerical and theoretical results of 2.50%. The results of the numerical simulation are consistent with the results of the theoretical calculation and indicate that the numerical method is sufficiently accurate to be used for the structural optimization analysis of the valve seat.
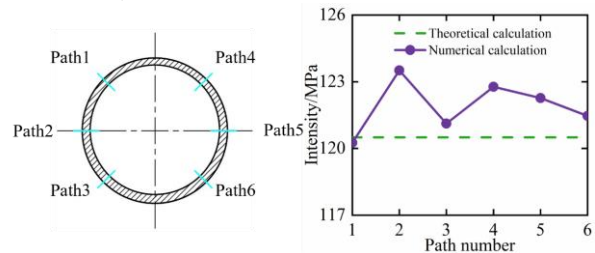

Fig. 5 Comparison between numerical results and theoretical results

3 Results and discussion

3.1 Temperature and stress analysis

Fig. 6 shows the temperature distribution of the valve seat when the HTHPV is closed. It can be seen from the figure that the surface temperature of the valve seat in contact with high-temperature air is the highest, and the temperature around the valve body is relatively lower, with a maximum temperature of

242.47 ℃ and a minimum temperature of 22 ℃. The temperature of the valve seat decreases from the direction of the central axis to the periphery. Because of the cooling structure, the temperature around the cooling structure is significantly lower than that further away, which shows that the cooling structure has a significant effect on the temperature of the valve seat. The temperature of the end face of the upper round groove is higher than that of the lower hole. In both the temperature near the central axis of the valve seat is higher while the temperature around it is lower.
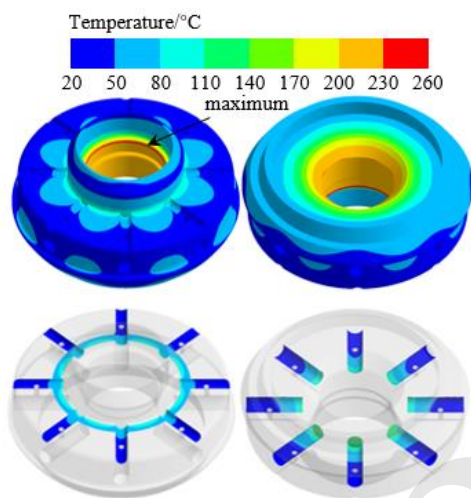
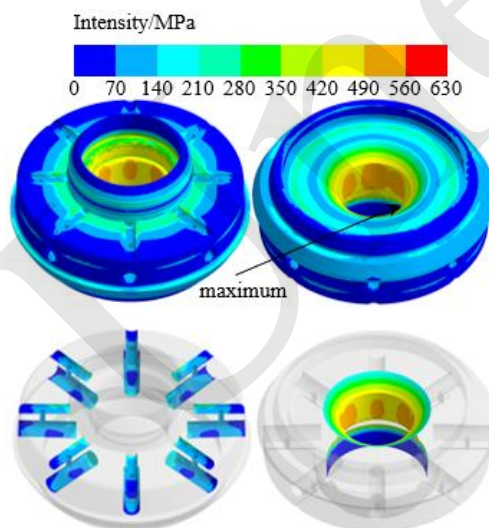**Fig. 6 Temperature distribution of the valve seat**

Fig. 7 Stress distribution of the valve seat

As shown in Fig. 7, the temperature gradient in the area in contact with high temperature gas is large. The thermal stress caused by the temperature gradient is also relatively large, which shows that the thermal

stress has a significant effect on the stress distribution in the valve seat. The trend of stress distribution in the valve seat is similar to that of the temperature distribution. The maximum stress appears in the center hole of the valve seat; its value is 624 MPa. The minimum stress occurs distant from the central hole, and the stress decreases from the central axis of the valve seat to the periphery. The cooling structure causes a stress concentration in the valve seat in this area, especially in the root area of the upper circular groove and the lower hole, which shows that the existence of the cooling structure leads to a weakening of the pressure bearing capacity of the valve seat.

3.2 Structural optimization analysis

Fig. 8 shows the local sensitivity of input parameters P_1–P_6 to output parameters P_7–P_{11}, and thus the variation of output parameters with input parameters. It can be seen from the figure that the parameter which has the greatest influence on the average temperature (P_7) is the distance from the end face of the lower hole to the Z-axis (P_4). The parameter which has the greatest influence on the average stress intensity (P_{11}) is the distance from the end face of the lower hole to the Z-axis (P_4). The diameter of the lower hole (P_5) and the distance from the axis of the lower hole to the origin of coordinates (P_6) both have significant effect on the average temperature (P_7). The distance from the end face of the lower hole to the Z-axis (P_4), and the diameter of the lower hole (P_5) and distance from the axis of the lower hole to the origin of coordinates (P_6) all have significant effect on the average stress intensity of the cooling surface for the valve seat (P_{13}).
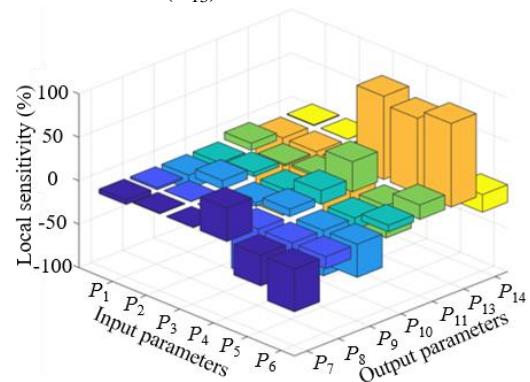

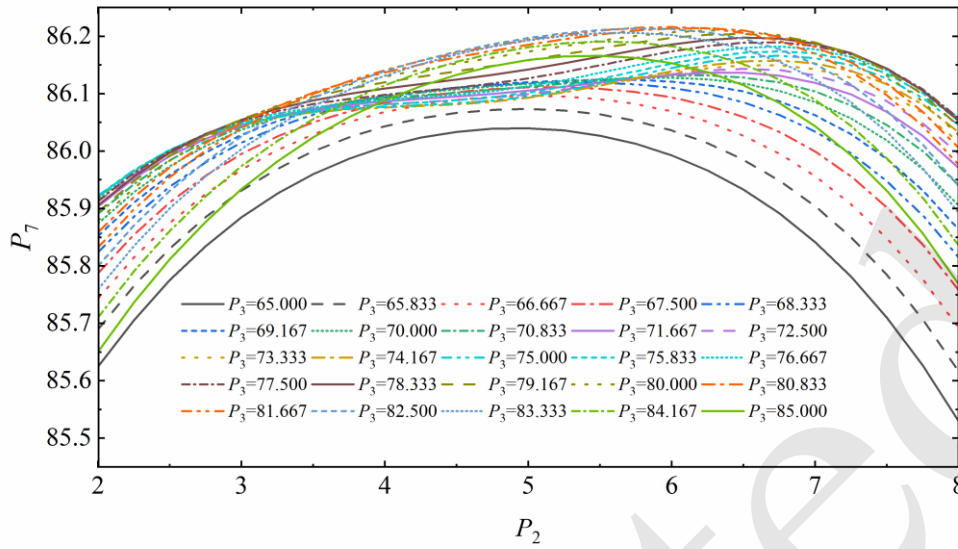**Fig. 8 Response of structural parameters to optimization objectives**

Fig. 9 Response of parameters P_2 and P_3 on optimization target P_7
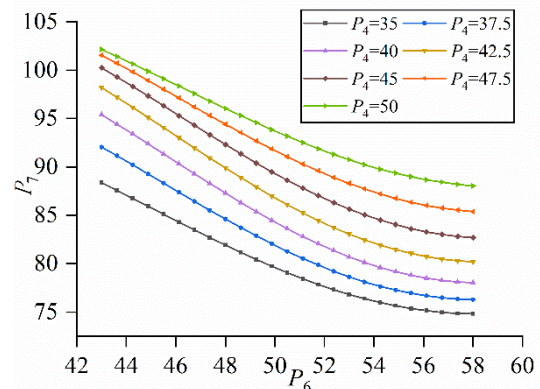
As shown in Fig. 9, when P_2 (diameter of the shear hole) changes from 2 mm to 8 mm, P_7 (average temperature of the valve seat) generally first increases and then decreases. With the change of P_2, when P_3 (distance from the center of the shear hole to Z-axis) is between 65 and 72.5 mm, P_7 generally first increases and then decreases; When parameter P_3 is between 72.5 and 80 mm, P_7 shows an "M-type" change trend; When P_3 is between 80 and 85mm, P_7 first increases and then decreases. When P_2 reaches a minimum or maximum value, the value of P_7 is small. With the continuous increase of P_3, the variation range of P_7 with P_2 increases. When $P_2 \leq 2$ mm or $P_2 \geq 7$ mm and $P_3 \geq 80$ mm, P_3 is relatively small, which provides a way to reduce the average valve seat temperature (P_7).

Fig. 10 illustrates the variation trend of P_7 (average temperature of the valve seat) with P_4 (the distance from end face of the lower hole to the Z-axis) and P_6 (the distance from the axis of the lower hole to the origin of the coordinates). When P_5 (diameter of the lower hole) remains unchanged, P_7 increases with the increase of P_4. When P_4 remains unchanged, P_7 decreases with the increase of P_5. Therefore, reducing P_4 and increasing parameter P_5 can effectively reduce the value of P_7. When P_4 remains unchanged, P_7 decreases with the increase of P_6. When $P_6 \leq 52$ mm, the decrease range of P_7 is large, and when $P_6 > 52$ mm, the decrease range of P_7 is small. When P_6 remains unchanged, P_7 also increases with the continuous increase of P_4. Therefore, increasing P_6 and

reducing P_4 can also effectively reduce the value of P_7.
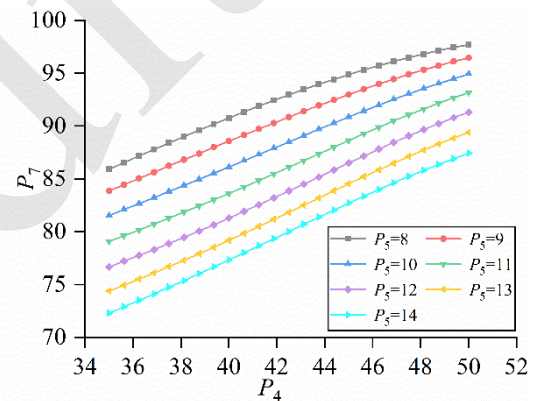
(a) Response of parameters P_4 on optimization target P_7

(b) Response of parameters P_6 on optimization target P_7
Fig. 10 Response of parameters P_4 and P_6 on optimization target P_7

As shown in Fig. 11, there is the response sur-

face of P_7 (average temperature of the valve seat) with P_1 (the diameter of the upper round groove) and P_2 (the diameter of the shear hole). When P_2 remains unchanged, P_7 decreases with the increase of P_1. When P_1 remains unchanged, P_7 first increases and then decreases with the increase of P_2. Therefore, increasing P_1 and $P_2 \leq 3$ mm or $P_2 \geq 7$ mm can reduce the value of P_7 slightly.

Fig. 12 indicates the variation trend of P_{11} (the average stress intensity of the valve seat) with P_1 (the diameter of the upper round groove) and P_2 (the diameter of the shear hole). When $P_2 \leq 5$ mm, P_{11} increases with the increase of P_1. When $P_2 \geq 5$ mm, P_{11} decreases first and then increases with the increase of P_1. It should be noted that when $P_{11} \leq 12.5$ mm, the change range of P_{11} is small, and when $P_{11} \geq 12.5$ mm, the change range of P_{11} is relatively large. When P_1 is small, the value of P_{11} increases with the increase of

P_2. When P_1 is large, the value of P_{11} decreases with the increase of P_2. Increasing the decreasing P_2 while reducing the P_1 can effectively reduce the value of P_{11}.
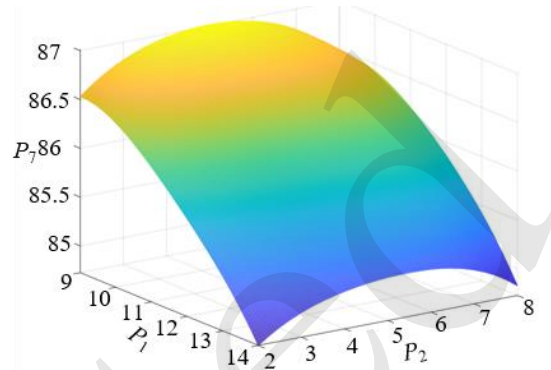

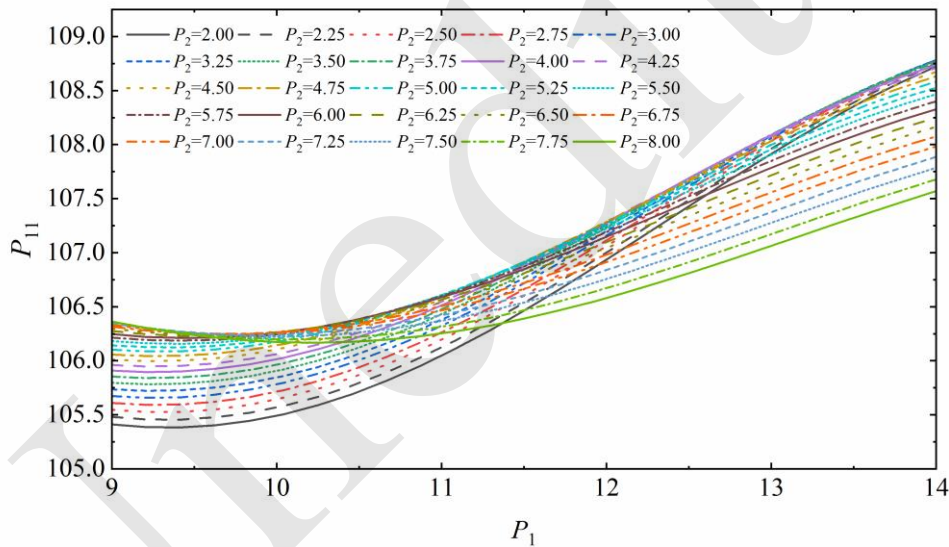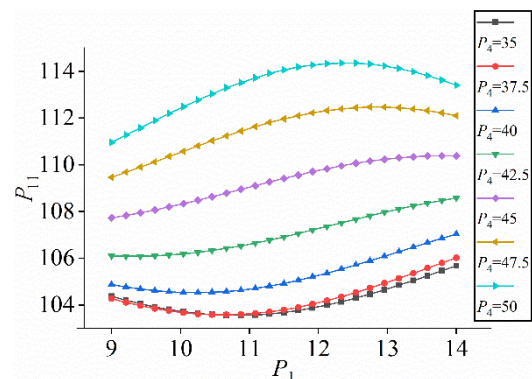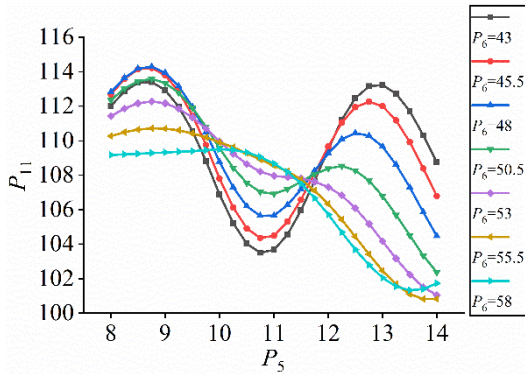**Fig. 11 Response of parameters P_1 and P_2 on P_7**

Fig. 12 Response of parameters P_1 and P_2 on optimization target P_{11}

Fig. 13 shows the variation trend of P_{11} (the average stress intensity of the valve seat) with P_1 (the diameter of the upper round groove) and P_5 (the diameter of the shear hole). When $P_4 \leq 40$ mm, and with the increase of P_1, parameter P_{11} first decreases and then increases. When $P_4 > 40$ mm, P_{11} first increases and then decreases the increase of P_1. When P_1 remains unchanged, P_{11} increases with the increase of parameter P_4. This shows that when P_1 is 11–12 mm and $P_4 \leq 10$ mm, the value of P_{11} can be effectively reduced. When $P_6 \leq 55.5$ mm, with the increase of P_5, P_1 also shows an M-type change trend, which shows

that when P_5=11 mm and $P_6 \leq 43$ mm, the value of P_{11} is the smallest.

(a) Response of parameters P_1 on optimization target P_{11}

(b) Response of parameters P_5 on optimization target P_{11}
Fig. 13 Response of parameters P_1 and P_5 on optimization target P_7

In Fig. 14, the response surface of P_{11} (the average stress intensity of the valve seat) with P_3 (the distance from the center of the shear hole to the Z-axis) and P_4 (the distance from end face of the lower hole to Z-axis) is shown. When P_3 remains invariable, P_{11} decreases with the increase of P_4. When P_4 remains unchanged, P_{11} increases with the increase of P_3. Therefore, the value of P_{11} can be reduced slightly by increasing P_4 and reducing P_5.
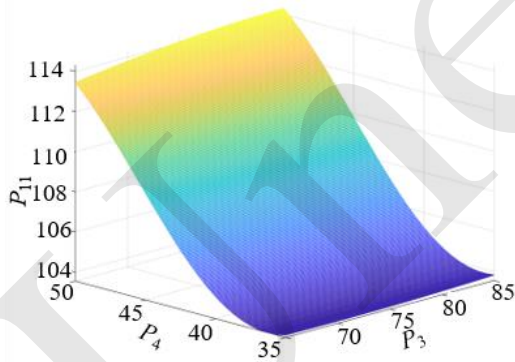

Fig. 14 Response of parameters P_3 and P_4 on optimization target P_7

Fig. 15 shows the response surface of P_{11} (the average stress intensity of valve seat) with P_2 (the diameter of the shear hole) and P_6 (the distance from the axis of the lower hole to the origin of the coordinates). When P_2 remains unchanged, parameter P_{11} decreases with the increase of P_6. When $P_6 \leq 50$ mm, P_{11} is augmented with the increase of parameter P_2. When $P_6 > 50$ mm, parameter P_{11} falls off with the increase of P_2. Therefore, increasing P_2 and decreas-

ing P_6 can reduce the value of P_{11} slightly.

At the values of P_1-P_6 shown in Table 4, the average temperature of the valve seat can be reduced from 242.47 ℃ to 70.61 ℃, and the average stress of the valve seat can be reduced from 115.22MPa to 100.02MPa, which shows that the cooling performance of the valve seat has been greatly improved and security is guaranteed.
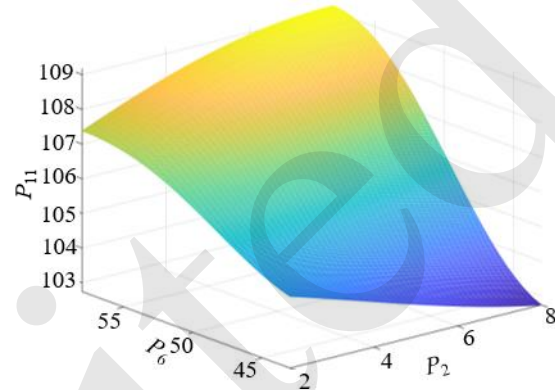

Fig. 15 Response of parameters P_2 and P_6 on optimization target P_7

Table 4 Optimization results of structural parameters for optimization value

Parameter	Initial value	Final value
P1	10 mm	11.90 mm
P2	5 mm	2.81 mm
P3	75 mm	74.78 mm
P4	47 mm	36.06 mm
P5	14 mm	13.83 mm
P6	58 mm	54.95 mm
P7	242.47 ℃	70.61 ℃
P11	115.22 MPa	100.02 MPa

5 Conclusions

When the HTHPV is closed, the temperature around the cooling structure is significantly lower than that away from the area due to the existence of the cooling structure. The temperature of the area in contact with high-temperature air is significantly higher than that of the surrounding area.

The stress distribution of the valve seat is similar to that of temperature. The maximum stress appears at the center hole of the valve seat, the minimum stress appears at the position far away from the center hole, and the stress distribution reduces from the center

axial direction of the valve seat. The existence of the cooling structure causes a stress concentration of the valve seat in this area, especially in the root area of the upper circular groove and the lower hole, which shows that the existence of the cooling structure weakens the pressure-bearing capacity of the valve seat.

An optimization method based on cooling structure parameters is proposed, which can completely describe the geometric characteristics of the cooling structure and improve cooling performance. Through the central composite design method and screening optimization method, the influence of various parameters on the optimization objective is analyzed. P_4 (the distance from end face of the lower hole to the Z-axis) has the most obvious effect on P_7 (average temperature of the valve seat). P_4 (the distance from end face of the lower hole to the Z-axis) and P_6 (the distance from the axis of the lower hole to the origin of coordinates) have the most obvious effect on P_{11} (the average stress intensity of valve seat). Finally an optimal design value is proposed in which the average temperature of the valve seat can be reduced from 242.47 ℃ to 70.61 ℃ and the average stress of the valve seat can be reduced from 115.22 MPa to 100.02 MPa.

Author contributions

Fengwei HOU designed the research. Haifeng SHU and Binbin WU processed the corresponding data. Wenqing LI wrote the first draft of the manuscript. Chengliang YU and Zhehui MA helped to organize the manuscript. Fengwei HOU and Jinyuan QIAN revised and edited the final version.

Conflict of interest

Fengwei HOU, Haifeng SHU, Binbin WU, Chengliang YU, Zhehui MA, Wenqing LI and Jinyuan QIAN declare that they have no conflict of interest.

References

Formato A, Guida D, Ianniello D, et al., 2018. Design of delivery valve for hydraulic pumps. *Machines*, 6(4):44.
https://doi.org/10.3390/machines6040044

Yu K, Xu JL, Zhang XF. et al., 2018. Starting characteristics and phenomenon of a supersonic wind tunnel coupled with inlet model. *Aerospace Science and Technology*, 77:626-637.
https://doi.org/10.1016/j.ast.2018.03.050

Shitol éB, 2020. Bolt strength in sectional body construction of valves. *Journal of Pressure Vessel Technology*, 142(3): 034502.
https://doi.org/10.1115/PVP2019-93775

Achuthan A, Jayanath S, 2021. Stress analysis of variable ram blowout prevention valves. *SPE Drilling & Completion*, 36(03):647-657.
https://doi.org/10.2118/205348-PA

Armijo KM, Mendoza H, Parish J, 2022. Vapor transport analysis of a chloride molten salt flow control valve. *In AIP Conference Proceedings*, 2445(1).
https://doi.org/10.1063/5.0085644

Zhou, X, Zhi XQ, Gao X, et al., 2022. Cavitation evolution and damage by liquid nitrogen in a globe valve. *Journal of Zhejiang University-SCIENCE A*, 23(2): 101-117.
https://doi.org/10.1631/jzus.A2100168

Aliyeva S, Abbasov S, 2023. Determination of the friction force between the draw rod and its guide in sucker rod well pumps and an analytical study of the stress deformation state of the valve assembly. *NAFRA-GAZ*, 36(01): 596-603.
https://doi.org/10.18668/NG.2023.09.05

Morales LD, Silva GP, Barros LDO, et al., 2023. Damage to fracture in offshore engineering materials under several stress states: Blowout preventer valve application. *Advances in Structural Engineering*, 26(11):2025-2054.
https://doi.org/10.1177/13694332231182862

Bryk M, Banaszkiewicz M, Kowalczyk T, et al., 2022. Slowly-closing valve behaviour during steam machine accelerated start-up. *Case Studies in Thermal Engineering*, 39:102457.
https://doi.org/10.1016/j.csite.2022.102457

Grice D, Hanke L, Mathias J, 2022. Analysis of Stop Valve Leaks: Environmental Stress Cracking of Styrene Copolymer Valve Stems. *Journal of Failure Analysis and Prevention*, 22(2):666-675.
https://doi.org/10.1007/s11668-022-01364-2

Shul'zhenko MG, Kolyadyuk AS, 2021. Thermal Strength of Steam Turbine Shut-Off and Control Valves Body. *Strength of Materials*, 53(6):877-888.
https://doi.org/10.1007/s11223-022-00355-w

Li JF, Xiao MQ, Sun Y, et al., 2020. Failure mechanism study of direct action solenoid valve based on thermal-structure finite element model. *IEEE Access*, 8:58357-58368.
https://doi.org/10.1109/ACCESS.2020.2982941

Sundararaj S, Krishnakumar P, Anirudh VR, et al., 2022. Effect of water pressure and temperature on spherical float of level sensing auto drain valve. *Materials Today: Proceedings*, 49:1490-1497.
https://doi.org/10.1016/j.matpr.2021.07.235

Qian JY, Xu JX, Zhong FP, et al., 2023. Solid-liquid flow characteristics and sticking-force analysis of valve-core fitting clearance. *Journal of Zhejiang Universi-*

ty-SCIENCE A, 24:1096-1105.
https://doi.org/10.1631/jzus.A2300061

Deng, X, 2022. Computational Analysis of Turbulence and Thermal Characteristics in Fluid Film Thrust Bearings (Doctoral dissertation, University of Virginia).

Jawwad AKA, Mahdi M, Alshabatat N, 2019. The role of service-induced residual stresses in initiating and propagating stress corrosion cracking (SCC) in a 316 stainless steel pressure-relief-valve nozzle set. *Engineering Failure Analysis*, 105:1229-1251.
https://doi.org/10.1016/j.engfailanal.2019.07.062

Bryk M, 2022. Thermal-strength analysis of a slow closing valve during accelerated startup of a steam turbine. *Journal of Power Technologies*, 102(2).

Hwang SY, Kim MS, Lee JH, 2020. Thermal stress analysis of process piping system installed on LNG vessel subject to hull design loads. *Journal of Marine Science and Engineering*, 8(11):926.
https://doi.org/10.3390/jmse8110926

Li WQ, Zhao L, Yue Y, et al., 2022. Thermo-mechanical stress analysis of feed-water valves in nuclear power plants. *Nuclear Engineering and Technology*, 54(3):849-859.
https://doi.org/10.1016/j.net.2021.09.018

Sun B, Zhao T, Kurnianto Prayitno YA, et al., 2021. Optimization of design variables for rotary regenerative thermal oxidizer high-temperature valve (rto-HTV) based on transient dynamics analysis and multi-objective optimization algorithm. *AIP Advances*, 11(12).
https://doi.org/10.1063/5.0075307

Fersaoui B, Cerdoun M, May A, 2022. Thermo-mechanical stress analysis within a steel exhaust valve of an internal combustion engine. *Proceedings of the Institution of Mechanical Engineers, Part C: Journal of Mechanical Engineering Science*, 236(1):635-654.
https://doi.org/10.1177/0954406221996394

Zhang H, Zhao L, Peng SE, et al., 2021. Thermal-fluid-structure analysis of fast pressure relief valve under severe nuclear accident. *Nuclear Engineering and Design*, 371:110937.
https://doi.org/10.1016/j.nucengdes.2020.110937

Jalali A, Delouei AA, 2019. Failure analysis in a steam turbine stop valve of a thermal power plant. *Engineering Failure Analysis*, 105:1131-1140.
https://doi.org/10.1016/j.engfailanal.2019.07.057

Liu QT, Yin FL, Nie SL, et al., 2021. Multi-objective optimization of high-speed on-off valve based on surrogate model for water hydraulic manipulators. *Fusion Engineering and Design*, 173:112949.
https://doi.org/10.1016/j.fusengdes.2021.112949

Bao YH, Wang HG, 2022. Numerical study on flow and heat transfer characteristics of a novel Tesla valve with improved evaluation method. *International Journal of Heat and Mass Transfer*, 187:122540.
https://doi.org/10.1016/j.ijheatmasstransfer.2022.122540

Kunčická L, Kocich R, 2022. Effects of Temperature (In) homogeneity during Hot Stamping on Deformation Be-

havior, Structure, and Properties of Brass Valves. *Advanced Engineering Materials*, 24(7):2101414.
https://doi.org/10.1002/adem.202101414

Li BB, Li RR, Liu XM, et al., 2022). Effects of operating parameters on flow force characteristics in a conical throttle valve. *Industrial Lubrication and Tribology*, 74(2): 251-257.
https://doi.org/10.1002/adem.202101414

Zong CY, Li QY, Li KP, et al., 2022. Computational fluid dynamics analysis and extended adaptive hybrid functions model-based design optimization of an explosion-proof safety valve. *Engineering Applications of Computational Fluid Mechanics*, 16(1):296-315.
https://doi.org/10.1080/19942060.2021.2010602

Wang HL, Chen XY, 2022. Optimization of micromixer based on an improved Tesla valve-typed structure. *Journal of the Brazilian Society of Mechanical Sciences and Engineering*, 44(4):143.
https://doi.org/10.1007/s40430-022-03454-6

Cao G, Wu HC, Chu YM, et al., 2022. Optimal design and dynamic optimization of the main pressure regulating valve for heavy-duty automatic transmission using GA and PSO algorithms. *Journal of the Brazilian Society of Mechanical Sciences and Engineering*, 44(3):94.
https://doi.org/10.1007/s40430-022-03370-9

Zhang TY, Zhou JZ, Yang X, et al., 2022. Multi-objective optimization and decision-making of the combined control law of guide vane and pressure regulating valve for hydroelectric unit. *Energy Science & Engineering*, 10(2):472-487.
https://doi.org/10.1002/ese3.1038

Lin ZH, Yu LJ, Hua TF, et al., 2022. Seal contact performance analysis of soft seals on high-pressure hydrogen charge valves. *Journal of Zhejiang University-SCIENCE A*, 23(4):247-256.
https://doi.org/10.1002/ese3.1038

Wang LT, Zheng SK, Liu X, et al., 2021. Flow resistance optimization of link lever butterfly valve based on combined surrogate model. *Structural and Multidisciplinary Optimization*, 64(6):4255-4270.
https://doi.org/10.1631/jzus.A2100395

中文概要

题　目：风洞用高温高压阀门阀座参数化设计研究

作　者：侯峰伟[1]，舒海峰[1]，吴斌彬[2]，于成亮[2]，马哲辉[3]，李文庆[4]，钱锦远[3]

机　构：[1]中国空气动力研究与发展中心，超高速所，中国绵阳，621000；[2]上海科科阀门集团有限公司，中国上海，201802；[3]浙江大学，能源工程学院，中国杭州，310027；[4]浙江大学，流体动力基础件与

机电系统全国重点实验室，中国杭州，310058

目　的： 风洞系统中高温高压介质会对热阀承压能力产生显著影响。本文旨在提出基于 MOGA 模型的阀门阀座参数化设计方法，探讨冷却结构参数对阀座承压能力和冷却能力的影响规律，建立适应性结构优化方法，为高温高压阀门设计提供参考。

创新点： 1. 设计了具有优良隔热能力的阀座冷却结构；2. 基于 MOGA 模型提出了阀座冷却结构参数化设计方法。

方　法： 1.通过理论分析的方式设计具有良好隔热能力的阀座冷却结构，验证其冷却能力；2.通过参数化建模建立阀座冷却结构的几何模型，关联冷却结构特征参数和几何模型特征；3.通过仿真模拟进行参数敏感性分析（图 8），提出基于 MOGA 模型的阀座冷却结构优化设计方法，建立优化的阀座冷却结构设计方案。

结　论： 1. 提出的冷却结构设计方法可完整地描述阀座几何结构的特征；2.阀座冷却结构竖孔的设计深度和位置对于阀座的应力状态和平均温度具有显著影响；3.优化后的阀座结构平均温度可从 242.47℃降低到 70.61℃，阀座的平均应力可从 115.22MPa 降低到 100.02MPa。

关键词： 热阀；风洞；应力；结构优化